ARTICLE NO. 78-1179

Locked Vortex Afterbodies

B.H. Little Jr.* and R.R. Whipkey†
Lockheed-Georgia Company, Marietta, Ga.

This research was concerned with the drag and flow characteristics of locked vortex afterbody shapes formed by thin disks spaced along a central spindle. Emphasis was placed on understanding such flows with an eye to developing drag reduction concepts for more conventional aircraft afterbodies. Experiments were performed to obtain 1) afterbody drag, 2) velocity and shear stress measurements around the bodies, and 3) flow visualization data in a low-speed smoke tunnel. A feature of these tests was the use of a two-component laser velocimeter for the velocity and shear stress measurements. The analysis centered on the development of criteria for low drag.

Nomenclature

$A\pi$ = cross-sectional area of body
C_D = drag coefficient
C_{P_G} = pressure coefficient in gap between forebody and afterbody
d = spindle diameter
D_0 = forebody diameter
D_1 = diameter of disk
P_G = pressure in gap between forebody and afterbody
P_∞ = static pressure from tunnel reference pitot tube
q_∞ = dynamic pressure from tunnel reference pitot tube
X = axial distance from body base to disk
t = thickness of disk
U_e = velocity at outer edge of shear layer
α = body angle of attack
u', v' = magnitudes of velocity fluctuations in x and y directions—defined as one standard deviation of the laser velocimeter histogram

Introduction

INTEREST in the possibility of utilizing vortex motion to aerodynamic advantage has intrigued aerodynamicists for a long time. Ringleb[1] pointed out that examples of such utilization occur in nature, and he went on to explore and describe applications in several areas of fluid flow design. Migay[2] tested such an application and was able to obtain improved diffuser efficiency in a ribbed diffuser that operated on a locked vortex principle. Recently, Roshko and Koenig[3] reported drag reduction of blunt forebodies by placing disks on spindles ahead of the body, and Mair[4] examined a similar physical concept for afterbody drag reduction.

While in none of the above (except Ringleb's work) do the authors place much emphasis on the locked vortex motion, Mair did establish that the low-drag regime was characterized by a relatively smooth vortex motion in the cavity formed between the body base and the trailing disk.

The Lockheed-Georgia Company has long been interested in applications of vortex flow control. Work was done in the 1960s on body contouring with locked vortices, and an ongoing program since 1964 has explored the spanwise blowing concept as applied to wings and control surfaces. In spanwise blowing, of course, a blowing jet is used to stabilize and augment vortex flows whose axes are oriented spanwise along the wing.

Presented as Paper 78-1179 at the AIAA 11th Fluid and Plasma Dynamics Conference, Seattle, Wash., July 10-12, 1978; submitted July 18, 1978; revision received Nov. 6, 1978.

Index categories: Configuration Design; Jets, Wakes, and Viscid-Inviscid Flow Interactions.

*Staff Scientist, Advanced Flight Sciences Dept.
†Sr. Aerodynamics Engineer, Advanced Flight Sciences Dept.

Afterbody drag has also been an area of concern at the Lockheed-Georgia Company where the main product for a number of years has been cargo aircraft. Cargo aircraft, with requirements for aft loading and airdrop, tend to have more afterbody drag than other types. A program was devised, therefore, to test afterbodies configured to utilize the locked vortex concept. Generally this program was an extension of Mair's work. Emphasis was placed, however, on physical modeling of the flow and on developing an understanding of such flows. It was the long-range objective that ideas and concepts might be gained which could be applied for drag reduction on aircraft afterbodies.

The scope of this work included three kinds of experiments. The first series of tests measured drag of locked vortex afterbodies; the second series was made in a smoke tunnel to obtain photographs of the smoke flow in and around the afterbody cavities; the third series utilized a two-component laser velocimeter (LV) to measure steady and unsteady velocity components around the afterbodies.

Apparatus and Methods

The wind tunnel used for the force and LV tests had a test section 18 in. wide by 30 in. high. It was an induction tunnel with good flow uniformity and a test section turbulence level of the order of 0.3%. The model installation, shown in Fig. 1, was established for testing primarily at zero angle of attack. Through manual adjustment of the model support, however, small changes in α were possible.

The model consisted of a 4-in.-diam rounded nose forebody and detachable afterbodies. The forebody, which was strut supported from the tunnel floor, contained an internal balance to measure axial and normal forces on the afterbody. An air gap was maintained between the fore and afterbody sections, and balance readings were corrected for the gap pressure—the pressure acting on the blunt forward face of the afterbody section. In all cases, the afterbody drag coefficient was computed as:

$$C_D = \frac{\text{balance readout}}{q_\infty A\pi} - \frac{P_G - P_\infty}{q_\infty}$$

The locked vortex or disk-and-spindle afterbody models are shown in Fig. 2. Two spindle diameters were tested—one ⅜-in. diameter ($d/D_0 = 0.0938$) and the other 1⅛-in. diameter ($d/D_0 = 0.281$). The disks were nominally 0.06 in. thick, although in one test a thicker disk, $t = 0.2$ in., was used.

No wind tunnel corrections were applied to these data. This is justified on the following basis: 1) configuration changes were not large, 2) all tests were made at zero attack angles, 3) all tests were made at the same freestream q, and 4) drag increments were used for evaluation of effects. The tunnel dynamic pressure was 12.5 psf. This equates to a freestream velocity of about 100 fps and a unit Reynolds number of 0.64×10^6/f.

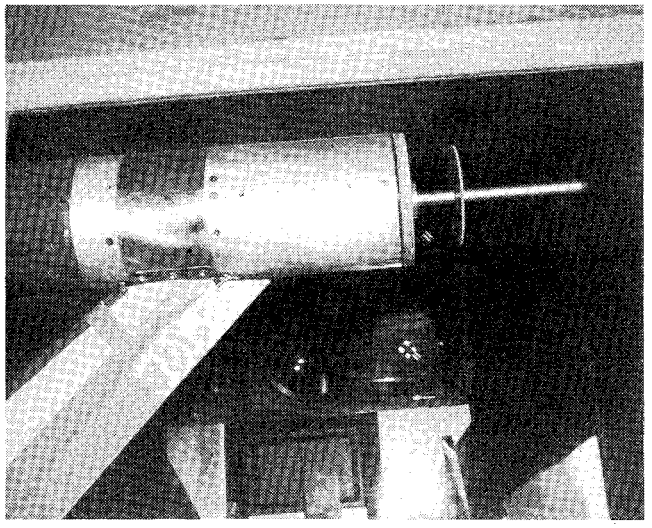

Fig. 1 Model in wind tunnel.

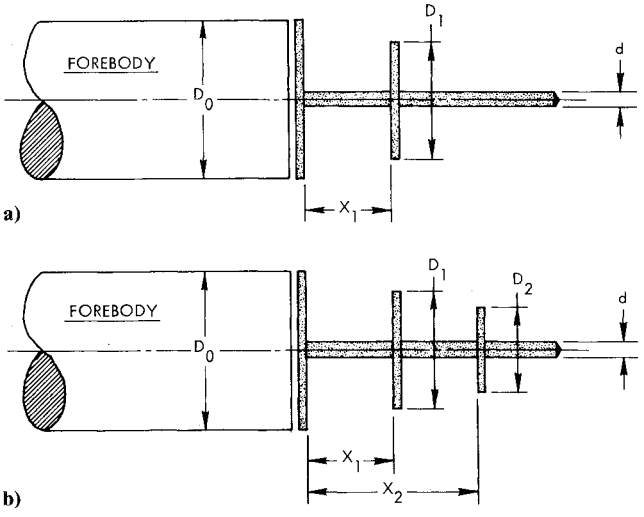

Fig. 2 Geometry of locked vortex afterbody arrangements. a) single disk; b) two disks.

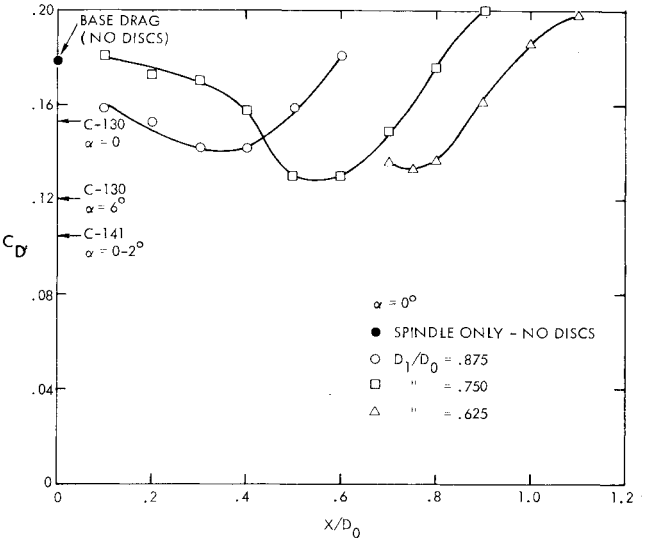

Fig. 3 Drag of single-disk afterbodies—large spindle.

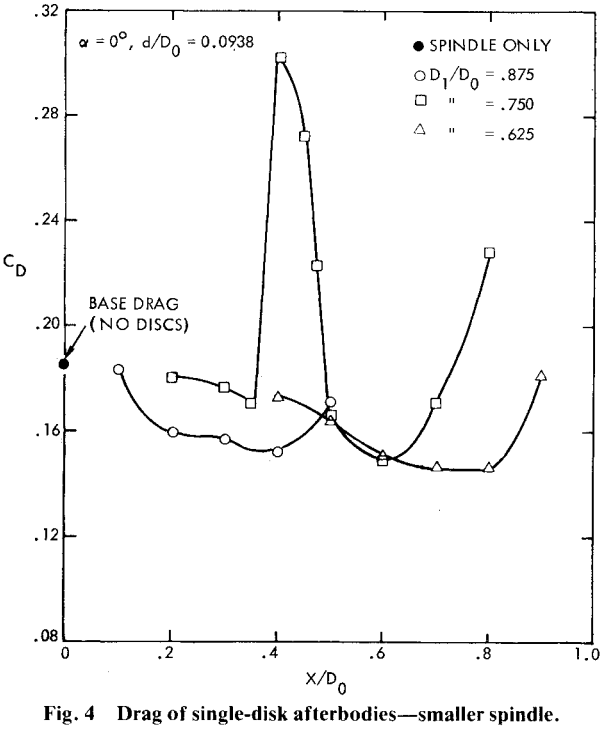

Fig. 4 Drag of single-disk afterbodies—smaller spindle.

The model used for smoke flow visualizations was 2 in. in diameter and the spindle was scaled to $d/D_0 = 0.0938$ to match the smaller spindle configuration of the force tests. Velocities in the smoke tunnel were of the order of 1 fps, so that the flow over and around the body was laminar.

Results

Drag Tests

Drag data for the larger diameter spindle ($d/D_0 = 0.281$) are shown in Fig. 3. For each disk diameter it can be seen that there is an optimum position, and also there is one combination of disk diameter and axial position that is optimum for the geometric variables tested. On the vertical scale of Fig. 3, the drag levels of several other configurations are shown for reference. The black dot shows base drag of the body and spindle alone. Arrows indicate drag of the C-130 afterbody shape at $\alpha = 0$ and 6 deg and the C-141 afterbody shape for $\alpha = 0$ to 2 deg. It can be seen that the best locked vortex arrangement has drag values ($C_D = 0.125$) comparable to the C-130 shape and not much greater than the C-141 shape.

For the smaller spindle (Fig. 4) drag is higher, and the best configuration is a smaller disk further downstream when compared to the larger spindle geometry. The most striking feature of Fig. 4, however, is perhaps the drag spike that occurs for $D_1/D_0 = 0.75$ in the X/D_0 range around 0.4. Mair[4] reported that the drag spike "was only found for values of D_1/D_0 between about 0.75 and 0.85." Our data would add to that restriction that the drag spike was not found for the larger spindle. So it appears that the drag spike phenomenon is one that only occurs in a certain range of cavity sizes, and that one might be able to eliminate such spikes, when they occur, by changing either the vertical or horizontal dimensions of the cavity.

Envelopes of minimum drag positions for various disk sizes are shown in Fig. 5. The drag data are presented in terms of ΔC_D with the no-disk base drag as a reference value. In this way a direct comparison can be made with Mair's data. A good bench mark is the correlation between data points at $X/D_0 = 0.6$ for the sharp-edge disks. Recognizing that Mair's spindle diameter ($d/D_0 = 0.125$) is slightly larger than ours ($d/D_0 = 0.094$), agreement between these drag points is quite good. Supporting the trend earlier noted, these data show drag to decrease as spindle diameter is increased. And, in accord with Mair's results, drag also decreases with rounding

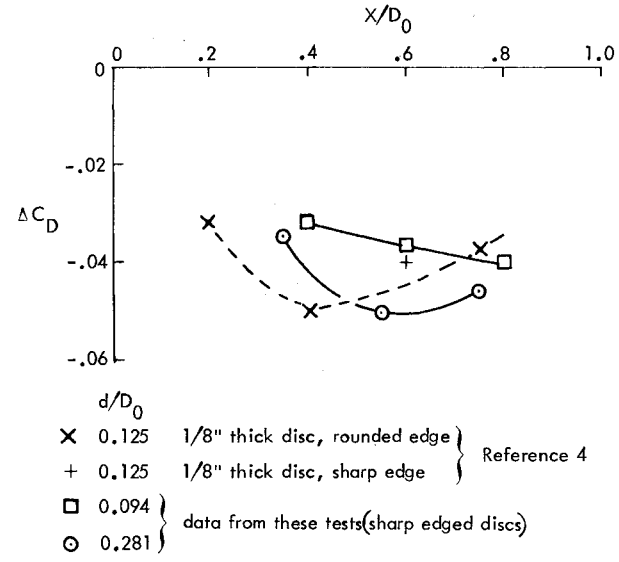

Fig. 5 Envelope of minimum drag conditions.

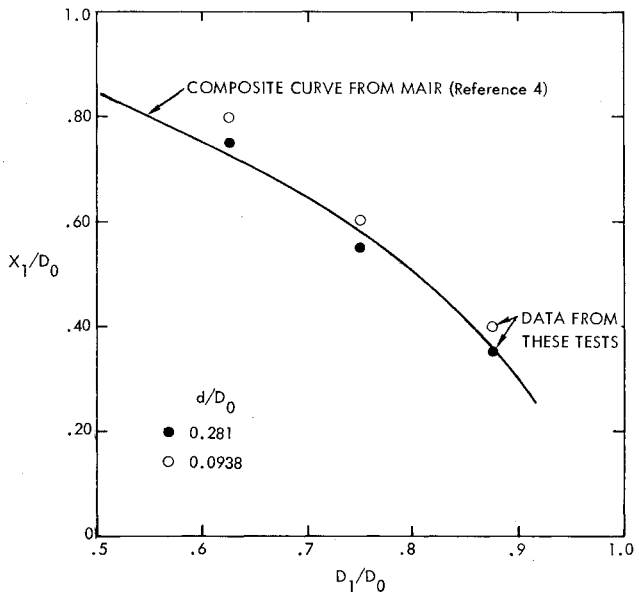

Fig. 6 Locus of disk geometries for minimum drag—single disks.

of the disk edges. Since it was not our objective to seek the optimum locked vortex configuration, but rather to explore the flow mechanisms involved, no attempt was made to further refine the design of such afterbodies.

In Fig. 6 is presented a plot of the X/D_0 position for minimum drag for varying disk diameters. The line shown represents a composite summary of Mair's data. Those data included the variables of disk thickness and disk edge rounding, but these had a secondary effect on drag. Likewise, it can be seen that our data show spindle diameter to have a secondary effect on drag, and in general our data agree well with those of Mair.

In contemplating how and where to explore the flow mechanisms involved in locked vortex afterbodies, it seemed advantageous to look at configuration where some obvious and dramatic changes occured. For our data, this naturally led to the selection of the geometry where the drag spike was encountered. This situation is examined in somewhat more detail than previously in Fig. 7, where the drag curve is shown for $D_1/D_0 = 0.750$ on the smaller spindle. The data points are reproduced on this curve, and for some of them the force balance output traces and the gap pressure values are presented.

Gap pressures, it may be recalled, are the pressures measured in the gap between the metric and nonmetric portions of the model. As explained in the section on apparatus, the afterbody drag was determined from the difference between the balance readout and the gap pressure term.

$$C_D = \frac{\text{balance readout}}{q_\infty A\pi} - \frac{P_G - P_\infty}{q_\infty}$$

It can be seen in Fig. 7 that the gap pressure forces are approximately equal for all disk positions except in the high-drag region of the drag spike. In those cases (points B and C) the gap pressures are almost 50% lower than for the other points shown. Since a lower pressure in this region is associated with a greater flow turning around the corner, it is inferred that this observation of lower pressure means that the flow in the drag spike region is overturning or turning too much inward in the base region. This will be examined further in the discussion of flow visualization and laser anemometer results.

The balance readout represents a summation of pressure forces on the cavity and aft surface of the disk. At point A there is a moderate drag load on these surfaces; at point B it is about three times as large; at point C it is back down to the point A level, but fluctuating wildly. These observations seem consistent with the inferences drawn from the pressure measurements, i.e., at point B there is too much turning of the flow and consequently too much impact drag load on the disk. At point C the flow is fluctuating in between a high-drag and low-drag condition. Point D shows that the balance readout has gone negative—there is a thrust load on the cavity and aft disk surfaces. At point E the disk is so far aft that it is picking up a drag load with the same amount of flow turning that was beneficial when the disk was further forward.

Flow Visualization Studies

The model for smoke tunnel flow visualization studies was one-half the size of the force model. With the very low velocity (of the order of 1 fps), the unit Reynolds number for the smoke tunnel tests was about 6000/f and the Reynolds number based on model diameter was about 1000. There should always be a question about the ability of tests at such low Reynolds numbers to simulate the flow patterns at high Reynolds numbers. When the dominant flow phenomena are controlled by viscous forces, there may be little similarity, but in the present situation, where the dominant flow phenomena involve separation at a sharp edge, viscous effects (and consequently Reynolds number differences) are not likely to be of prime importance.

The smoke tunnel photographs for the $D_1/D_0 = 0.75$ disk size and a series of disk positions are shown in Figs. 8-14. For the no-disk case (Fig. 8) the wake stays broad near the body but tends to close rather abruptly at about $X/D \approx 1.7$. With the disk at $X/D_0 = 0.2$ (Fig. 9) there appears to be little effect on the flow near the base, but wake closure is perhaps less abrupt. This trend toward less abrupt wake closure continued to develop as a general pattern when the disk is moved farther and farther aft, although it requires some careful examination of those photographs to pick this out. Tracings were made of the wake boundaries shown in the photographs and these are reproduced in Fig. 15. These tracings show the aft wake closure position to move downstream as the disk is moved downstream to $X/D_0 = 0.6$. Beyond that point, further downstream disk movement seems to reverse the trend. The closure for $X/D_0 = 0.7$ is upstream of that for $X/D_0 = 0.6$.

There are some other interesting things to be noted from the smoke tunnel photographs. No locked vortices are apparent in the cavities until X/D_0 is increased to 0.3. The vortex in this case, however, is caused by reversed flow moving upstream and shedding as it flows over the edge of the disk. The vortex in Fig. 10 in the lower part of the cavity is rotating clock-

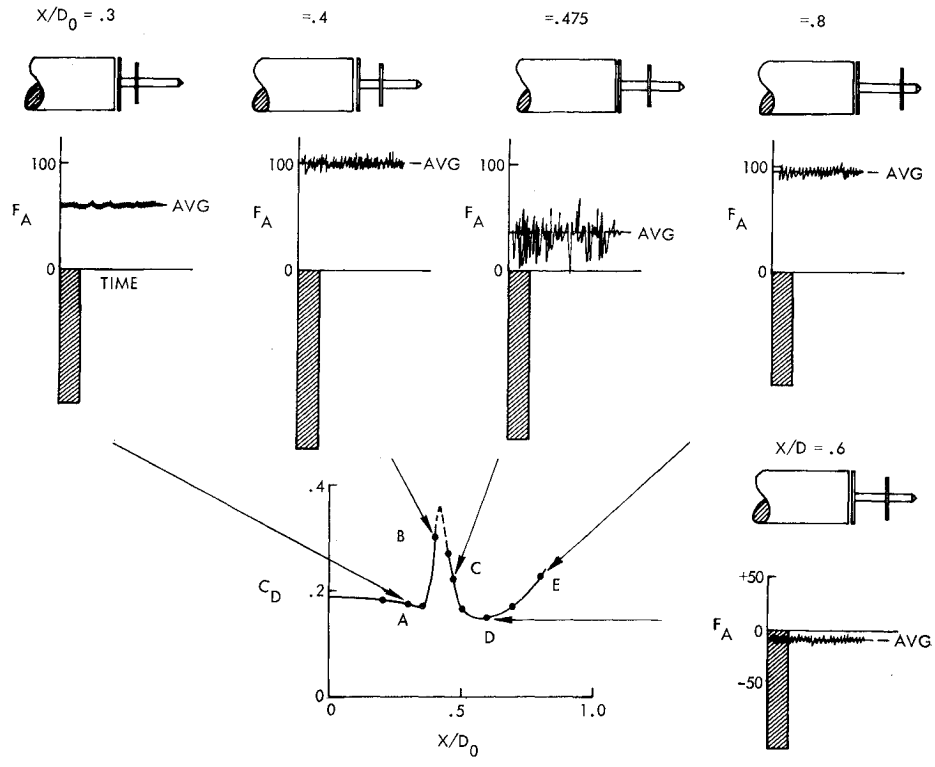

Fig. 7 Relationship of drag "spike" to flow unsteadiness.

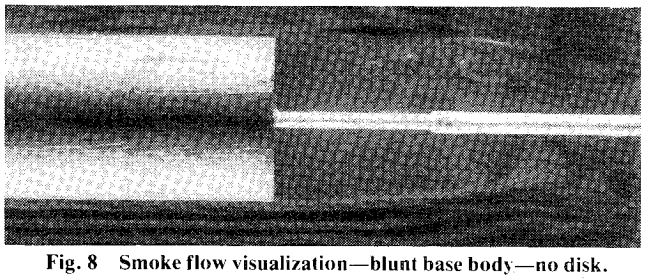

Fig. 8 Smoke flow visualization—blunt base body—no disk.

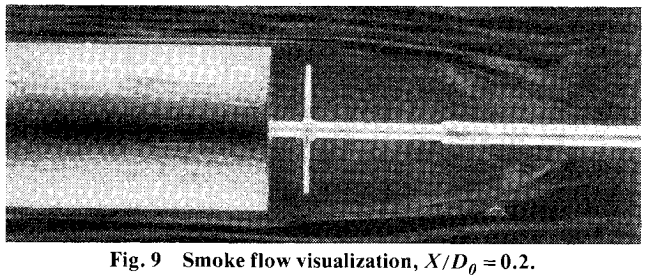

Fig. 9 Smoke flow visualization, $X/D_0 = 0.2$.

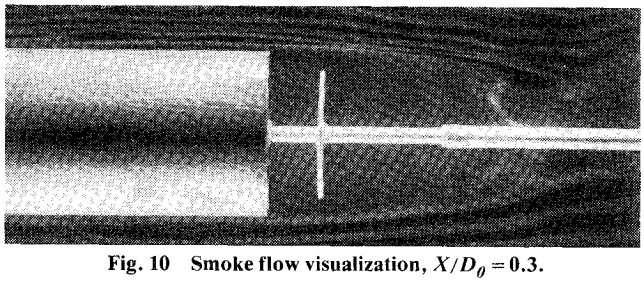

Fig. 10 Smoke flow visualization, $X/D_0 = 0.3$.

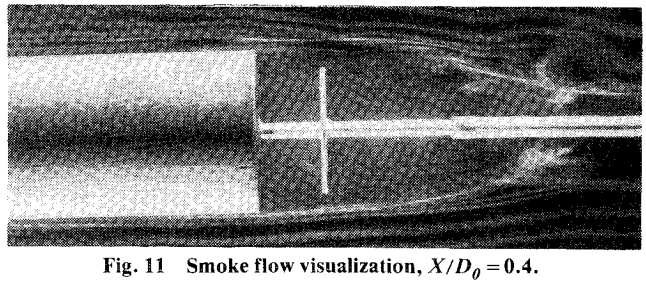

Fig. 11 Smoke flow visualization, $X/D_0 = 0.4$.

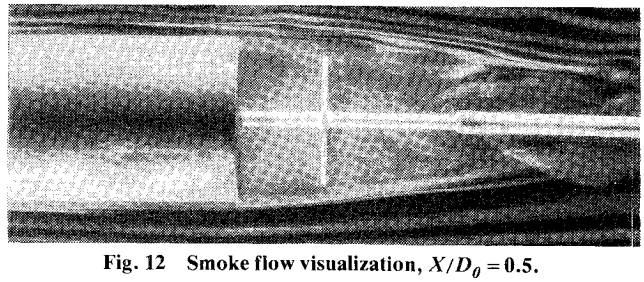

Fig. 12 Smoke flow visualization, $X/D_0 = 0.5$.

wise—shed by the wake back flow. (This observation will be confirmed by examination of the laser velocimeter results.) For $X/D_0 = 0.4$ (Fig. 11) the vortex is now shed by the mainstream moving past the base of the body. Looking next at Fig. 13 we see a beautifully developed cavity vortex at $X/D_0 = 0.6$—appearing to be a progressive development from the flow shown for $X/D_0 = 0.4$ (Fig. 11). At $X/D_0 = 0.5$ (Fig. 12), however, there really is no definable vortex. This is in the region where the flow is very unsteady. Again the laser velocimeter measurements are needed to throw light on this situation.

Two things should be noted about the smoke tunnel flow for $X/D_0 = 0.6$. First the flow was stable in the vortex cavity. The vortical flow could be oberved to rotate slowly and smoothly. When the smoke was turned off and the tunnel permitted to run on, it could be noted that the cavity smoke gradually bled out into the wake region. At other X/D_0 disk positions, mass transfer rates into and out of the cavity, as determined by this technique, were much higher. Second the vortex seems better sized to the cavity than in the $X/D_0 = 0.4$ case or in the $X/D_0 = 0.7$ case (Fig. 14). And, of course, it should be noted that this smooth vortical flow occurs for the X/D_0 position which gave minimum drag in the force tests.

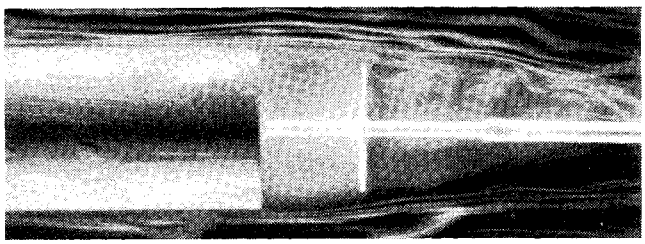

Fig. 13 Smoke flow visualization, $X/D_0 = 0.6$.

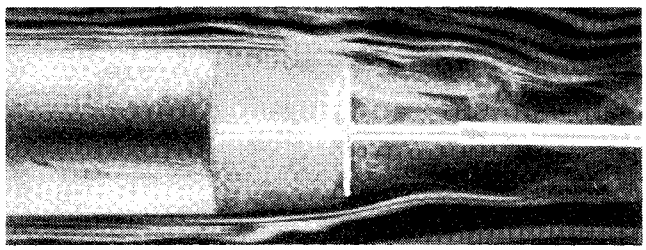

Fig. 14 Smoke flow visualization, $X/D_0 = 0.7$.

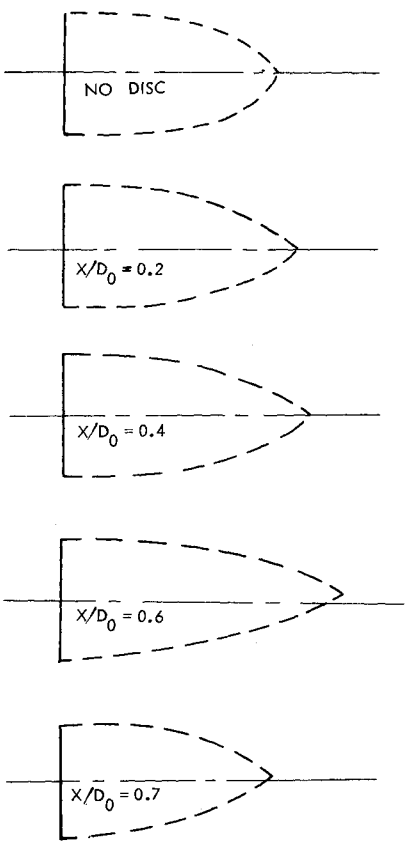

Fig. 15 Tracings of wakes from smoke flow photographs.

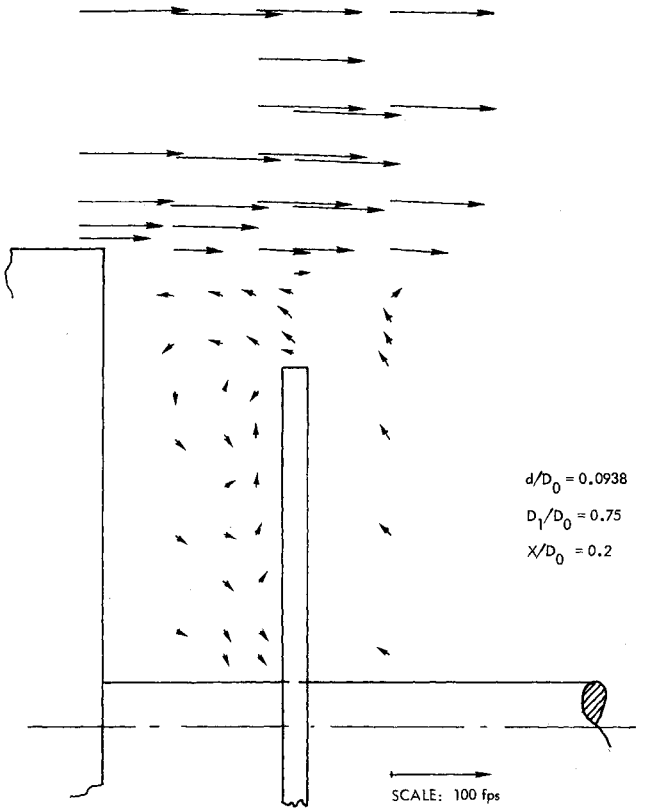

Fig. 16 LV velocity vectors, $X/D_0 = 0.2$.

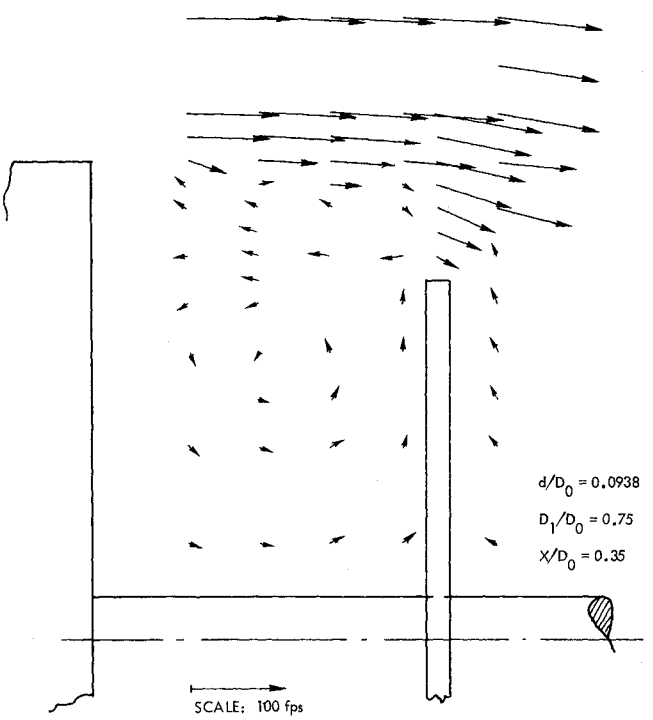

Fig. 17 LV velocity vectors, $X/D_0 = 0.35$.

Laser Velocimeter Measurements

Figures 16 through 19 show mean velocity vectors for the $D_1/D_0 = 0.75$ disk at various positions on the smaller spindle ($d/D_0 = 0.0938$). These velocity vectors were taken in the vertical centerline plane. Figure 16, for $X/D_0 = 0.2$, shows quite clearly the backflow over the disk, which results in a vortex flowing counter to the mainstream flow. (The corresponding smoke flow picture is in Fig. 10.) This yields a new concept of the disk as a device for limiting the size of the dead water region of the wake—or a device for inhibiting wake backflow.

Figure 17, for $X/D_0 = 0.35$, appears to be a composite representing two flow modes—one in which there is backflow over the disk and a second in which the flow is apparently contracting around the disk.

At $X/D_0 = 0.45$ the velocity vectors depict a flow contracting around the disk, but in this disk position the flow at the disk edge is inclined inward too much for smooth flow either upstream or downstream of the disk. Upstream of the disk there is a strong vortical flow, and downstream there is a strong divergence of flow away from the centerline. By contrast Fig. 19, for $X/D_0 = 0.6$, shows the disk to be in a

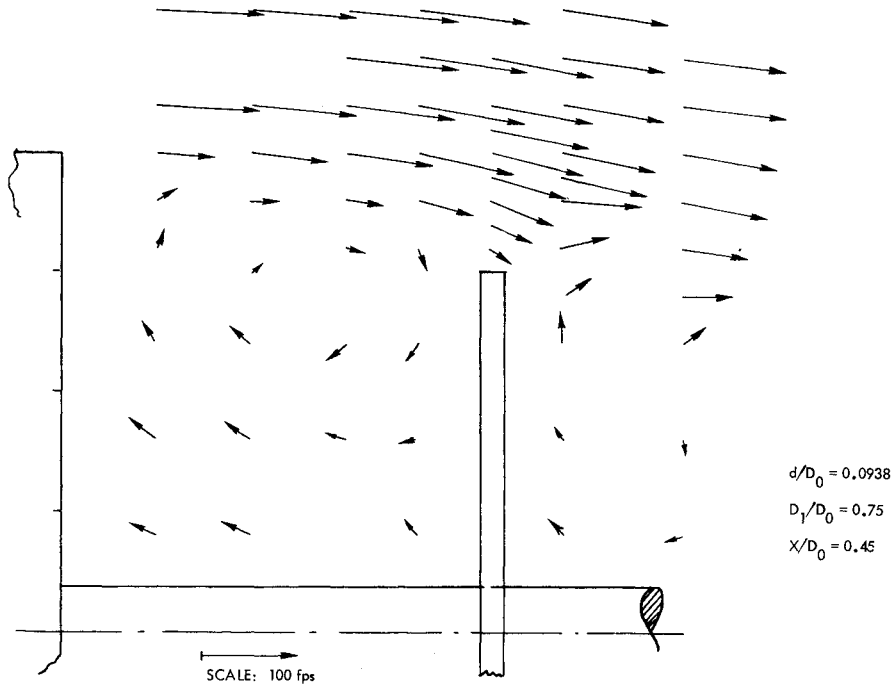

Fig. 18 LV velocity vectors, $X/D_0 = 0.45$.

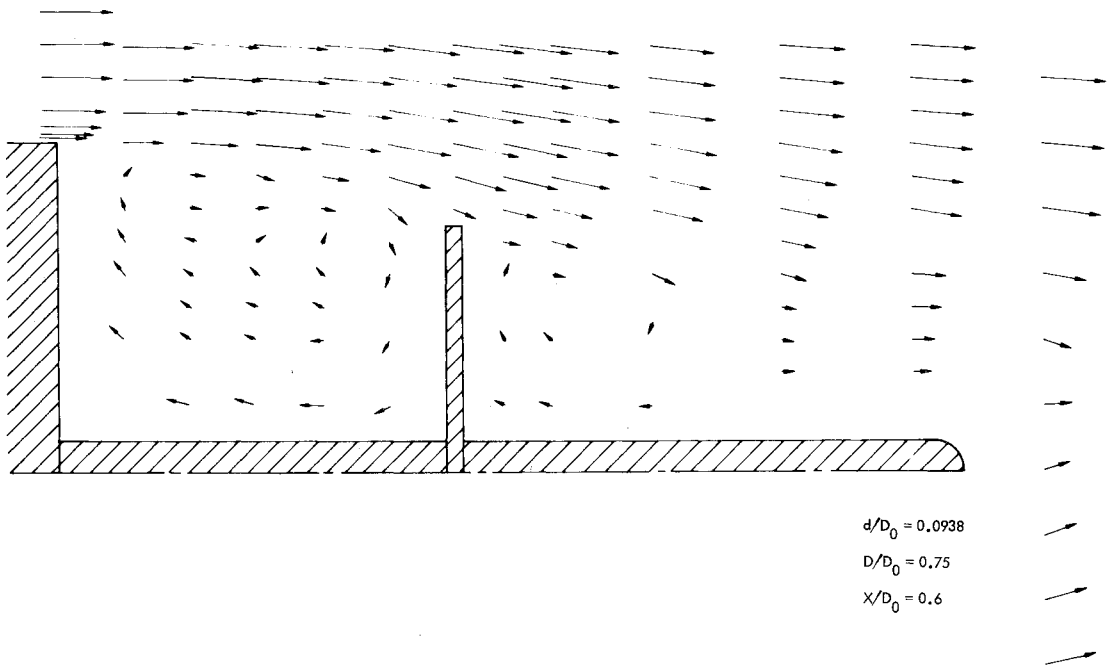

Fig. 19 LV velocity vectors, $X/D_0 = 0.6$.

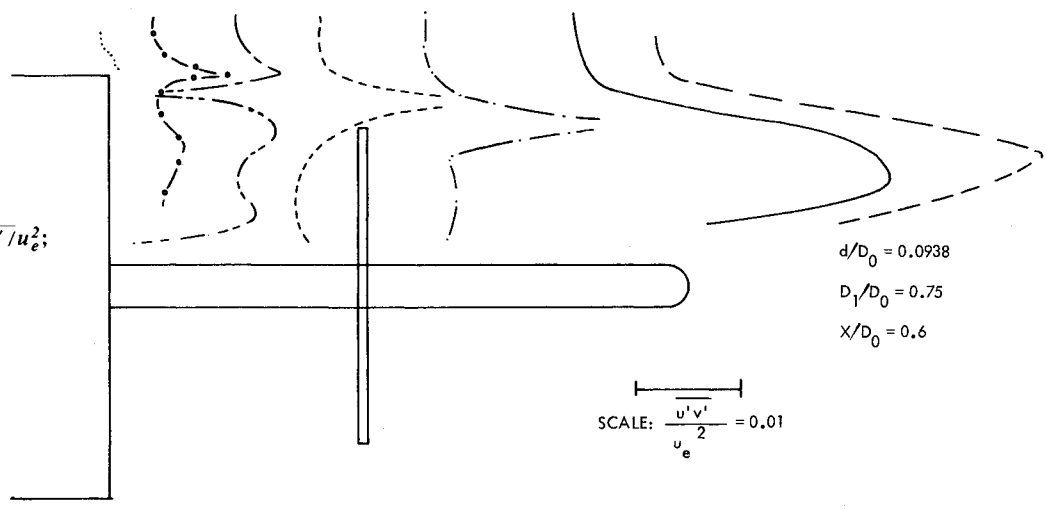

Fig. 20 Shear stress term, $\overline{u'v'}/u_e^2$; for low-drag configuration.

much better position with smooth flow fore and aft. There is a smaller percentage of the cavity flow whirling at high velocity, and the mainstream flow goes smoothly past the disk with little or no readjustment of flow direction downstream of the disk.

There are several interesting things to be noted about these laser velocimeter pictures of the flow. First perhaps is the excellent agreement between the smoke tunnel portrayals of flow patterns and the quantitative depictions by the LV. In several important respects these two techniques agree. There is a backflow vortex spilling over the edge of the disk at $X/D_0 = 0.2$, which is shown in Fig. 10 for smoke flow visualization and in Fig. 16 for the LV. The smoke flow for $X/D_0 = 0.5$ (Fig. 12) and the LV flow vectors plot for $X/D_0 = 0.45$ (Fig. 18) look remarkably alike, with a small vortical cell in the upper-right-hand corner of the cavity. Finally, there is the smooth low-drag condition at $X/D_0 = 0.6$ portrayed by smoke flow in Fig. 13 and by the LV in Fig. 18. In this last pair of figures both flow portrayals show the vortical flow nicely filling the cavity with a relatively smooth outer flow around the disk.

In summarizing the results from drag, flow visualization, and laser velocimeter measurements, the following regimes are established.

Wake Backflow Regime

The flow is dominated by a backflow in the body wake. Disks placed close to the body base inhibit this backflow. If the disk is sufficiently smaller than the base, the backflow spills upstream over the edge of the disk and creates a vortex rotating with edge velocity opposing the freestream velocity. A low-drag disk at these close-to-the-base positions must be large enough so that this upstream spillover does not occur.

Cavity Vortex Regime—Unsteady Flow

Moving the disk downstream from the position where wake backflow predominates, or increasing disk diameter at these close-in positions causes the flow to shift into a mode where the wake backflow does not move upstream past the disk. Then a cavity vortex is formed with outer edge velocities moving downstream. This can be a very unsteady flow with the mainstream first contracting to impinge on the edge of the disk, thus trapping too much air in the cavity, and consequently expanding to permit some of the trapped air to escape from the cavity. In this regime the vortex is not centered in the cavity, but appears to be too small for the cavity. The load on the drag balance shows the flow fluctuating from a low- to high-drag condition.

Cavity Vortex Regime—Steady Flow

At some combination of disk diameter, disk position, and spindle diameter, the cavity vortex centers itself fairly well in the cavity and produces a smooth cavity flow and external flow. This corresponds to the minimum-drag condition. Mass transfer into and out of the cavity is minimized. In the smoke tunnel this was measured by permitting the cavity to fill with smoke and then turning the smoke off. In the minimum-drag configuration the smoke would rotate slowly in the cavity for times of the orders of 10 s before dissipating. In badly nonoptimum configurations the dissipation time was of the order of 1 s.

If the disk is moved downstream beyond the optimum location, the smoke tunnel photographs show that once more the vortex size and cavity size are mismatched. Too much air impinges on the disk and drag begins to rise.

Shear Stress Measurements

The two-component laser velocimeter permits measurement of the shear stress term $\overline{u'v'}/u_e^2$. In an incompressible flow this parameter is one-half of the local shear stress. Shear stress data were collected for all LV measurement positions, but only the data for the optimum disk position on the smaller spindle are shown in Fig. 20. Such data are not easy to validate since there is little in the way of theory or other experiments for such flows. However, the wall shear stress in the boundary layer approaching the base should be about 0.004 (based on Re_θ measured in the boundary layer there). The LV measured values appear quite consistent with this predicted value. Another comparison can be made with jet flow data[5-7] where maximum values of $\overline{u'v'}/u_e^2$ in the jet mixing region of approximately 0.02 are quite common. Therefore, the values shown in Fig. 20 appear to be at about the right level. They are presented here for information. The complete set of these data will be examined in detail in a later work.

Concluding Remarks

The combination of test techniques used in this program—force measurements, smoke tunnel flow visualization, and laser velocimeter measurements—has provided a good physical description of the flow over locked vortex afterbodies. It has been demonstrated that in order to reduce drag, the disk or other device defining the downstream boundary of the locked vortex cavity must be large enough to separate the wake backflow from the cavity flow so that a locked vortex can exist in the cavity. Furthermore, the cavity thus formed must have dimensions such that the locked vortex effectively fills the cavity. This then appears to be the key to defining optimum locked vortex geometries—to define the cavity dimensions for a given flow which will match the smooth stable vortex.

The value of low-velocity smoke tunnels in helping to define flow patterns and establish optimum flow conditions has certainly been well demonstrated by these tests. Similarity between photographs from the smoke tunnel and velocity vector plots from the laser velocimeter measurements show remarkable agreement.

These tests also speak well for the laser velocimeter as a flow-diagnostic tool. There are enough points of good correlation between the LV measurements and other observations to lend confidence that both mean velocity and shear stress in flows, such as the one studied, have been adequately described.

References

[1] Ringleb, F. O., "Separation Control by Trapped Vortices," *Boundary Layer and Flow Control,* edited by G. V. Lachmann, Pergamon Press, N.Y., 1961, pp. 265-294.

[2] Migay, V. K., "Study of Ribbed Diffusers" (in Russian), *Toploenergetika,* No. 10, 1962. English translation issued as A. R. C. Paper 25,382, 1963.

[3] Roshko, A. and Koenig, K., "Interaction Effects on the Drag of Bluff Bodies in Tandem." Presented at the Symposium on Aerodynamic Drag Mechanisms of Bluff Bodies and Road Vehicles, General Motors Research Laboratories, Sept. 27-28, 1976.

[4] Mair, W. A., "The Effect of a Rear-Mounted Disc on the Drag of a Blunt-Based Body of Revolution," *The Aeronautical Quarterly,* Nov. 1965, pp. 350-360.

[5] Lau, J. C. and Morris, P. J., "Turbulence Measurements in Subsonic and Supersonic Jets Using a Laser Velocimeter," AIAA Paper 76-348. Presented to the 9th Fluid and Plasma Dynamics Conference, San Diego, Calif., July 14-16, 1976.

[6] Sami, S., Carmody, T., and Rouse, H., "Jet Diffusion in the Region of Flow Establishment," *Journal of Fluid Mechanics,* Vol. 27, Pt. 2, 1967, pp. 231-252.

[7] Wygnanski, I. and Fiedler, H., "Some Measurements in the Self Preserving Jet," *Journal of Fluid Mechanics,* Vol. 38, Pt. 3, 1969, pp. 577-612.